# Multi-omics reveals the mechanism of Trimethylamine N-oxide derived from gut microbiota inducing liver fatty of dairy cows

Chenlei Li[1,2†], Feifei Wang[1,2†], Yongxia Mao[1,2], Yanfen Ma[1,2] and Yansheng Guo[1,2*]

## Abstract

**Background** Trimethylamine N-oxide (TMAO) is a metabolite produced by gut microbiota, and its potential impact on lipid metabolism in mammals has garnered widespread attention in the scientific community. Bovine fatty liver disease, a metabolic disorder that severely affects the health and productivity of dairy cows, poses a significant economic burden on the global dairy industry. However, the specific role and pathogenesis of TMAO in bovine fatty liver disease remain unclear, limiting our understanding and treatment of the condition. This study aims to construct a bovine fatty liver cell model using an integrated approach that combines transcriptomic, proteomic, and metabolomic data. The objective is to investigate the impact of TMAO on lipid metabolism at the molecular level and explore its potential regulatory mechanisms.

**Results** We established an in vitro bovine fatty liver cell model and conducted a comprehensive analysis of cells treated with TMAO using high-throughput omics sequencing technologies. Bioinformatics methods were employed to delve into the regulatory effects on lipid metabolism, and several key genes were validated through RT-qPCR. Treatment with TMAO significantly affected 4790 genes, 397 proteins, and 137 metabolites. KEGG enrichment analysis revealed that the significantly altered molecules were primarily involved in pathways related to the pathology of fatty liver disease, such as metabolic pathways, insulin resistance, hepatitis B, and the AMPK signaling pathway. Moreover, through joint analysis, we further uncovered that the interaction between TMAO-mediated AMPK signaling and oxidative phosphorylation pathways might be a key mechanism promoting lipid accumulation in the liver.

**Conclusions** Our study provides new insights into the role of TMAO in the pathogenesis of bovine fatty liver disease and offers a scientific basis for developing more effective treatment strategies.

**Keywords** TMAO, Dairy cow hepatocyte, Lipid metabolism, Multi-omics, AMPK signaling pathway

[†]Chenlei Li and Feifei Wang contributed equally to this work.

*Correspondence:
Yansheng Guo
guoyansheng1978@163.com
[1]College of Animal Science and Technology, Ningxia University, Yinchuan 750021, China
[2]Key Laboratory of Ruminant Molecular and Cellular Breeding of Ningxia Hui Autonomous Region, College of Animal Science and Technology, Ningxia University, Yinchuan 750021, China

Li *et al. BMC Genomics*       (2025) 26:10

Page 2 of 17

## Introduction

The liver, as the primary metabolic organ in animals, plays a pivotal role in regulating energy balance and metabolic pathways [1–4]. Lipid metabolism is one of the critical physiological processes within hepatocytes and is closely linked to overall energy equilibrium and health status [5, 6]. For dairy cows, lipids constitute the main form of energy storage. During lactation, cows require substantial energy to maintain high levels of milk production. Hepatocytes modulate lipid metabolism to ensure a balance between energy supply and demand, with the efficiency of this metabolic process determining the synthesis and secretion of milk fat, thereby directly influencing the lactational performance of dairy cows [7, 8]. The periparturient period, spanning from 21 days before to 21 days after parturition, is a critical phase for dairy cows. Marked reductions in feed intake, coupled with the surge in energy requirements for the onset of lactation, lead to a state of negative energy balance (NEB) [9]. Studies have shown that NEB triggers extensive mobilization of body fat, precipitating metabolic disorders such as ketosis and fatty liver [10, 11].

The gut-liver axis plays a crucial role in the pathogenesis of non-alcoholic fatty liver disease (NAFLD), with gut microbiota and their metabolic products having profound effects on liver metabolic functions [12]. Notably, TMAO, whose precursor trimethylamine (TMA) is generated by gut microbiota through the metabolism of choline, L-carnitine, and phosphatidylcholine, is subsequently converted into TMAO in the liver by flavin-containing monooxygenases (FMO1 and FMO3) [13]. TMAO significantly influences the progression of NAFLD through the gut-liver axis. Studies indicate that TMAO is closely associated with an increased risk of cardiovascular diseases and regulates lipid metabolism by interfering with cholesterol metabolism, lipoprotein metabolism, and fatty acid oxidation [14–21]. This, in turn, inhibits the bile acid signaling pathway of the farnesoid X receptor (FXR) [22], leading to lipid accumulation in the liver of mice. Additionally, TMAO can exacerbate hepatic inflammation by boosting the release of inflammatory cytokines, which aggravates hepatocyte injury. Furthermore, TMAO promotes the development of NAFLD in mice fed a high-fat diet (HFD) by modulating glucose metabolism and increasing insulin resistance [23]. These mechanisms suggest that TMAO, by modulating the gut-liver axis, not only exacerbates the pathological progression of NAFLD but may also facilitate the transition to more severe liver conditions such as non-alcoholic steatohepatitis (NASH). Currently, research on TMAO in cattle is relatively limited, while studies in humans provide an important theoretical foundation. Although extrapolating human research findings to cattle involves certain limitations, this cross-species reference can offer valuable insights into the potential mechanisms of TMAO in cattle. Understanding these interactions is critical for developing new therapeutic strategies for NAFLD.

In recent years, with the rapid advancement of high-throughput sequencing technologies, omics-based research methods such as transcriptomics, proteomics, and metabolomics have been widely applied in the fields of biomedical and agricultural sciences, providing powerful tools to uncover various physiological regulatory mechanisms. For instance, Liu et al. identified six central genes potentially involved in the production of TMAO-activated hepatic cell exosomes (TMAO-Exos) through transcriptomic analysis of the exosomes (Exos) released by TMAO-Exos [24]. In the study by Lin et al., proteomic techniques revealed that anti-atherosclerotic could effectively reduce plasma TMAO levels in mice and slow the progression of atherosclerosis by modulating the composition of gut microbiota [25]. Utilizing metabolomics, Chen et al. discovered that TMAO interacts with and triggers the signaling pathway of the endoplasmic reticulum stress kinase (PERK), thus revealing the central roles of TMAO and PERK in the pathogenesis of metabolic syndrome and suggesting that modulation of the gut microbiota or inhibition of TMAO synthesis could reduce disease risk [26].Most research on TMAO to date has focused on human health, particularly in relation to cardiovascular diseases and lipid metabolism disorders. However, studies on lipid metabolism in bovine liver cells, particularly in the context of fatty liver disease, have been relatively limited, often concentrating on a single omics dimension rather than on the impact of TMAO. Therefore, this study aims to employ multi-omics approaches and integrative multi-omics analysis strategies to comprehensively and deeply investigate the effects and mechanisms of TMAO on liver metabolism in dairy cows.

This study integrates transcriptomic, proteomic, and metabolomic data, employing a joint analysis approach to elucidate the effects of TMAO on lipid metabolism in bovine hepatic cells. It aims to further our understanding of the relationship between TMAO and hepatic lipid metabolism, offering novel insights into the regulatory mechanisms of lipid metabolism in dairy cows.

## Materials and methods

### Culture and treatment of bovine hepatic cells

Dairy cow hepatic cells, kindly provided by Professor Yanfen Ma from Ningxia University, were adjusted to a seeding density of $1 \times 10^6$ cells/mL and inoculated into T75 culture flasks. The culture medium consisted of Dulbecco's Modified Eagle Medium (DMEM, c11995500BT, Thermo Fisher Scientific, Beijing, China) supplemented with 10% fetal bovine serum (FBS, 1099−141, Thermo

Li *et al. BMC Genomics*        (2025) 26:10

Page 3 of 17

Fisher Scientific, Australia) and 1% penicillin-streptomycin. Cells were cultured at 37 °C in an atmosphere containing 5% $CO_2$. Upon reaching approximately 80% confluence, the cells were randomized into two groups using a computer-generated sequence to ensure unbiased allocation. One group served as the control, while the other was designated for TMAO treatment. The cells were switched to serum-free DMEM and cultured for an additional 12 h. Subsequently, the original medium was removed, and the control group was replenished with fresh complete medium, while the TMAO treatment groups received complete medium containing 100, 200, 300, and 400 µmol/L TMAO (T833724-1 g, Macklin Biochemical Co., Ltd., Shanghai, China), respectively, for 12 h before cell pellets were collected. The obtained cell pellets were initially preserved in liquid nitrogen for 30 min and then stored at -80 °C for long-term preservation for subsequent experimental use. To achieve a more accurate depiction of cellular metabolism and related processes, we concentrated on intracellular analysis. RNA sequencing, proteomic, and untargeted metabolomics analyses were carried out on the cell samples.

### Assessment of liver injury and lipid metabolism biochemical markers, and oil red O staining experiment

The collected cell pellets were disrupted using an ultrasonic cell disruptor. Levels of aspartate aminotransferase (AST), alanine aminotransferase (ALT), and triglycerides (TG) in the samples were measured according to the instructions of biochemical assay kits (microplate method; AST: C010-2-1, ALT: C009-2-1, and TG: A110-1-1, Nanjing Jiancheng Bioengineering Institute, Nanjing, China). Subsequently, lipid droplets were stained using the Oil Red O staining kit (C0158S, Beyotime Biotechnology, Shanghai, China). The collected samples were fixed in 10% neutral formalin and then dehydrated using graded alcohols. Following rehydration, samples were stained with freshly prepared Oil Red O solution for 15 min. Excess stain was removed by washing with 60% isopropanol, and the samples were then counterstained with hematoxylin. Stained samples were mounted with glycerol gelatin and examined under a microscope to observe and quantify lipid droplets [27].

### Transcriptomic sequencing and analysis

RNA sequencing services were provided by Shanghai Biotechnology Corporation (Shanghai, China). Total RNA was extracted from collected cell samples using the Trizol method (CW0580, Kangwei Century Biotech Co., Ltd., Jiangsu, China). For this study, a total of 6 samples were used, consisting of 3 biological replicates for each of the two treatment conditions. The samples were selected to pilot both the adequacy of RNA extraction and the sequencing depth for our experimental setup. Briefly,

samples were homogenized in Trizol reagent, followed by phase separation with chloroform, RNA precipitation with isopropanol, and washing with ethanol. The RNA pellets were dissolved in RNase-free water. The quality and concentration of the extracted RNA were evaluated using a NanoDrop spectrophotometer (Thermo Scientific) to ensure adequate purity (A260/A280 ratio between 1.8 and 2.0) and integrity was verified using agarose gel electrophoresis. The mRNA was enriched from total RNA using Oligo(dT) magnetic beads to target polyA-tailed RNA. The enriched mRNA was fragmented into approximately 300 bp segments using ion fragmentation. First-strand cDNA synthesis was performed using the fragmented RNA as a template, 6-base random primers, and reverse transcriptase. The second-strand cDNA was synthesized using the first-strand cDNA as a template. Following cDNA synthesis, library construction involved PCR amplification to enrich library fragments, selecting for a final library size of approximately 450 bp. Libraries were then quality-checked using an Agilent 2100 Bioanalyzer to verify size distribution. Sequencing of the libraries was subsequently performed on the NovaSeq 6000 platform (Illumina).

Raw sequencing data in FASTQ format were filtered using Cutadapt software (v1.15). The filtered reads were then aligned to the bovine genome Bos taurus, specifically using the ARS-UCD1.2 version provided by Ensembl 109, with the HISAT2 tool (v2.0.5) [28]. To quantify gene expression levels, HTSeq (v0.9.1) was employed to tally the read count for each gene, serving as the initial expression measure [29]. These expression levels were then normalized using the FPKM (Fragments Per Kilobase of transcript per Million mapped reads) method. Principal component analysis (PCA) of gene expression levels within the transcriptome was conducted using the Omicshare data analysis platform (https://www.omicshare.com, accessed on 8 June 2023), developed by GENE DENovo, with default parameters. Identification of differentially expressed genes was performed using the DESeq (v1.30.0) R package, with a selection criteria of |log2FoldChange| > 1 and FDR < 0.05 [30]. Clustering analysis of gene expression patterns between samples was carried out using the Pheatmap package (v1.0.8) in R, with results presented as heatmaps [31] Differentially expressed genes were annotated using the KEGG database (http://www.kegg.jp/) [32], and their enrichment was analyzed using the ClusterProfiler package (v3.4.4) [33].

### Proteomic sequencing and analysis

Proteomic analysis services were provided by Shanghai Biotechnology Corporation (Shanghai, China). Proteins were extracted from cell samples utilizing an SDT lysis buffer composed of 4% SDS, 100 mM DTT, and 100

Li *et al. BMC Genomics*        (2025) 26:10

Page 4 of 17

mM Tris-HCl at pH 8.0. For this study, a total of 6 samples were analyzed, with 3 biological replicates for each of the two treatment conditions. We performed proteomic analysis on the same set of samples used in the transcriptomics analysis to maintain consistency across these two OMICS datasets. The samples underwent a boiling process for 5 min, followed by ultrasonication, and were subsequently boiled for an additional 5 min. Insoluble cellular debris was discarded after centrifugation at $16,000 \times g$ for 15 min. The resulting supernatant was collected and its protein concentration was quantified employing a BCA Protein Assay Kit (Bio-Rad, USA). For each sample, 200 μg of protein was digested using the FASP (Filter-Aided Sample Preparation) method as described by Wisniewski et al. The peptides were then purified using a C18 StageTip in preparation for LC-MS analysis [34]. The peptide concentrations were measured at OD280 using a Nanodrop One spectrophotometer.

LC-MS/MS analyses were conducted using a Q Exactive Plus mass spectrometer interfaced with an Easy 1200 nLC system (Thermo Fisher Scientific). The mass spectrometry data were processed and analyzed utilizing MaxQuant software (v1.6.0.16) [35]. Within the MaxQuant software, protein quantification ratios were weighted and normalized based on the median ratio [36]. PCA of protein expression levels was carried out using the Omicshare data analysis platform (accessed on June 2023). The identified proteins were evaluated in terms of fold change (FC) and p-value through the label-free quantification (LFQ) values, and proteins were selected based on an upregulation expression multiple of ≥2 and a p-value<0.05. Differentially expressed proteins were annotated and subjected to significant enrichment analysis using the KEGG database [37].

### Untargeted metabolomics sequencing and analysis
Untargeted metabolomics analysis services were provided by Shanghai Biotechnology Corporation (Shanghai, China). For metabolomics analysis, a total of 12 samples were used, consisting of 6 biological replicates for each of the two treatment conditions. This larger sample size was chosen to capture a broader spectrum of metabolites and ensure sufficient statistical power. Collected cell samples were homogenized with 1 mL of pre-cooled methanol/acetonitrile/water (v/v/v, 2:2:1), followed by ultrasonication in an ice-water bath for 1 h, and then incubated at -20 °C for 1 h to precipitate proteins. It is important to note that these metabolomics samples included the same set of initial 3 samples used in transcriptomics and proteomics, plus an additional 3 samples to enhance the robustness of metabolite detection. The samples were centrifuged at $14,000 \times g$ and 4 °C for 20 min, after which 800 μL of the supernatant was transferred to a sampling tube. The extracts were then vacuum-dried and reconstituted in 50% acetonitrile, filtered through a disposable 0.22 μm cellulose acetate filter, and transferred to 2 mL HPLC vials for storage at -80 °C. Metabolomic analysis was performed using a UPLC-ESI-Q-TOF-MS system (UHPLC, Shimadzu Nexera X2 LC-30AD, Shimadzu, Japan) coupled with a Q-Exactive Plus (Thermo Scientific, San Jose, USA).For liquid chromatography (LC) separation, samples were analyzed on an ACQUITY UPLC® HSS T3 column (2.1×100 mm, 1.8 μm) (Waters, Milford, MA, USA). The flow rate was maintained at 0.3 mL/min with mobile phase components consisting of A: 0.1% formic acid in water and B: 100% acetonitrile (ACN). The gradient program initiated with 0% buffer B for 2 min, increased linearly to 48% over 4 min, then ramped up to 100% in the next 4 min and held for 2 min, before returning to 0% buffer B in 0.1 min, followed by a 3-minute re-equilibration period. Electrospray ionization (ESI) was employed in both positive and negative ionization modes for separate MS data acquisition.

Multivariate data analysis and modeling were conducted using R (v4.0.3) and the ropls package (v1.36.0). Models were constructed employing PCA and orthogonal projections to latent structures-discriminant analysis (OPLS-DA) [38]. OPLS-DA facilitated the identification of metabolites with discriminative potential through variable importance in projection (VIP) scores, with significant differential metabolites being selected based on VIP≥1 and either FC>1.5 or FC<0.667, coupled with $P<0.05$. The selected differential metabolites were subjected to cluster analysis using R, and key differential metabolites were analyzed for KEGG pathway enrichment using the KEGG database to construct relevant metabolic pathways. To systematically investigate metabolic alterations, the abundance of differential metabolites was used to analyze the overall trends within metabolic pathways. Annotation results of differential metabolites were quantified using the DA score, with the top 30 pathways graphically represented.

### Integrated transcriptomic, proteomic, and metabolomic analysis
We conducted a comprehensive integration of transcriptomic, proteomic, and metabolomic data to identify key differential genes, proteins, and metabolites closely associated with the induction of fatty liver, guided by the enrichment analysis results of KEGG pathways ($P<0.05$). We utilized Cytoscape software (v3.10.1) to construct a multi-omics functional network diagram [39]. The correlation analysis was conducted using the OmicShare tool (accessed on June 2023). Specifically, we performed pairwise correlation analyses among the differentially expressed genes, proteins, and metabolites involved in the system network diagram. We applied stringent thresholds of |cor| > 0.9 and $P<0.01$ to select significant

correlations. The selected genes, proteins, and metabolites were then used to construct a correlation network diagram using Cytoscape software (v3.10.1). Ultimately, we synthesized the multi-omics data to illustrate a model depicting the potential impact of TMAO on lipid metabolism in bovine hepatic cells, and the mechanism diagram was created using Figdraw (https://www.figdraw.com). A detailed analysis workflow is provided in Supplementary Figure S5.

### qRT-PCR

The reliability of the transcriptomic data was verified using qRT-PCR to measure the expression levels of genes related to lipid metabolism. Gene primer sequences were synthesized by Sangon Biotech Co., Ltd. (Shanghai, China) (Supplementary Table S1). The acquired qRT-PCR data were analyzed using the $2^{-\Delta\Delta CT}$ method to calculate the relative gene expression levels.

### Statistical analysis

In our statistical analysis, data were initially organized and screened using Excel to ensure accuracy and completeness. Subsequently, we utilized GraphPad Prism software (v8.0) to perform in-depth analyses of quantitative data [40], specifically focusing on *SREBF1*, *MO25* and *AMPK* levels. Using this software, we applied ANOVA for comparisons of means across multiple groups, followed by Duncan's test to evaluate significant differences between groups. Statistical differences were considered significant at $P<0.05$ and highly significant at $P<0.01$.

## Result

### The impact of TMAO on bovine hepatic cell damage and lipid droplet accumulation

In this study, we investigated the effects of various concentrations of TMAO on bovine hepatic cells. The extent of liver cell damage inflicted by TMAO was assessed by measuring the intracellular content of AST, ALT, and TG. The experimental results indicated that TMAO led to

an increase in AST, ALT, and TG levels across all tested concentrations (Fig. 1). Notably, at concentrations of 200 μmol/L, 300 μmol/L and 400 μmol/L, there was a significant increase in AST levels compared to the control group ($P<0.05$, Fig. 1A). Concurrently, ALT and TG levels significantly increased after treatment with different concentrations of TMAO ($P<0.05$, Fig. 1B and C). These data suggest that TMAO can cause hepatic cell damage at various concentrations, with the most significant increase in liver cell damage and TG content observed at 400 μmol/L.

To further elucidate the impact of TMAO on lipid accumulation in hepatic cells, we conducted Oil Red O staining on liver cells treated with 400 μmol/L TMAO. The control group's bovine hepatic cell nuclei appeared dark blue with sparse red lipid droplets scattered in the cytoplasm (Fig. 2A). After treatment with 400 μmol/L TMAO, numerous dispersed red lipid droplets were observed in the hepatic cell cytoplasm (Fig. 2B), further substantiating that TMAO at 400 μmol/L significantly promoted the accumulation of lipid droplets in bovine hepatic cells. In summary, TMAO exerts a clear damaging effect on bovine hepatic cells at certain concentrations, with its impact on lipid metabolism being particularly pronounced at a concentration of 400 μmol/L. Subsequent omics studies are thus focused on investigating the effects of 400 μmol/L TMAO on liver metabolism.

### Identification and comparison of differentially expressed genes

PCA based on expression levels was performed on the samples, and the results showed that biological replicates within the same experimental group clustered together significantly (PC1: 66.5% and PC2: 11.5%), while samples from different experimental groups were clearly separated along PC1, confirming the stability and reliability of the sequencing results in this experiment (Fig. 3A). Further differential analysis identified a total of 4790 significantly
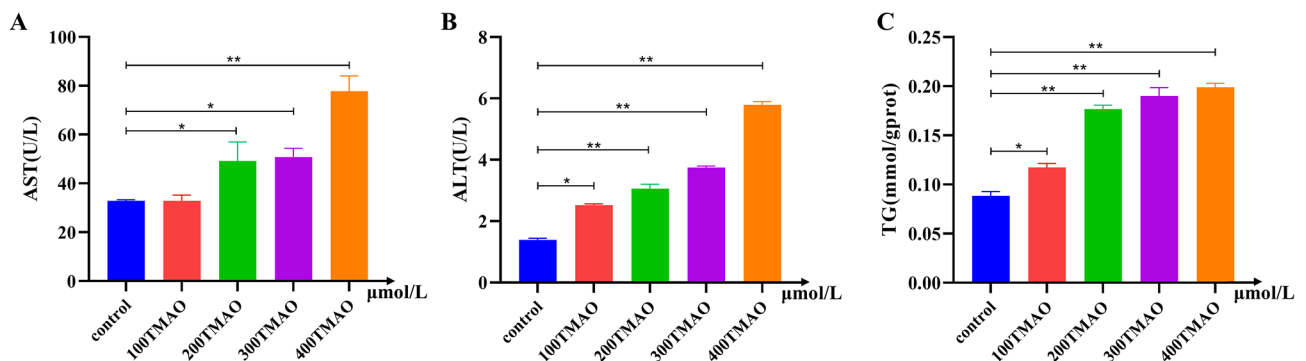


**Fig. 1** The effects of TMAO on the levels of AST, ALT, and TG in bovine hepatic cells. (**A**) Changes in AST levels under treatment with different concentrations of TMAO. (**B**) Changes in ALT levels under treatment with different concentrations of TMAO. (**C**) Changes in TG levels under treatment with different concentrations of TMAO. Compared to the control group, * indicates $P<0.05$, ** indicates $P<0.01$
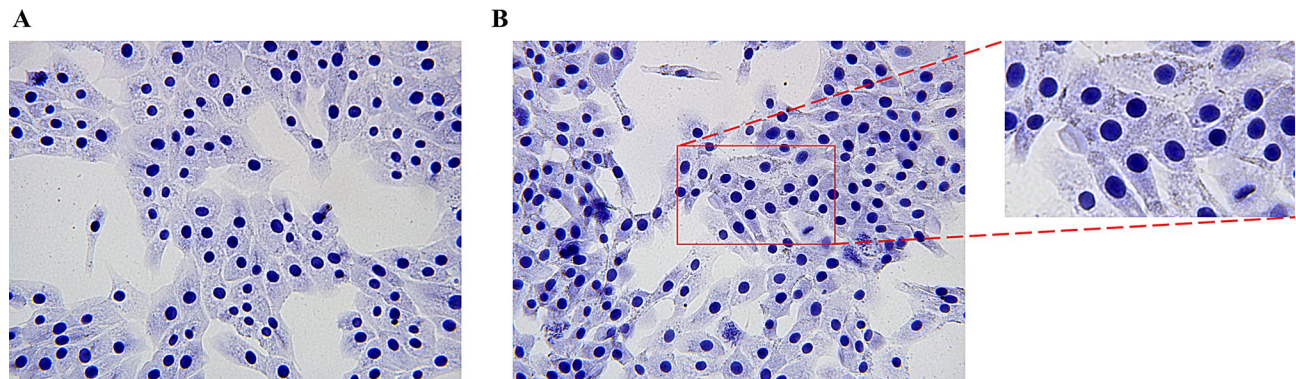
Li *et al. BMC Genomics*          (2025) 26:10

Page 6 of 17



**Fig. 2** Oil Red O staining illustrating the effect of TMAO treatment on lipid accumulation in bovine hepatic cells. (**A**) Oil Red O staining of control group bovine hepatic cells. (**B**) Oil Red O staining of bovine hepatic cells treated with 400 μmol/L TMAO. Oil Red O staining is used to visualize the accumulation of intracellular lipid droplets, with the red areas representing lipid droplets
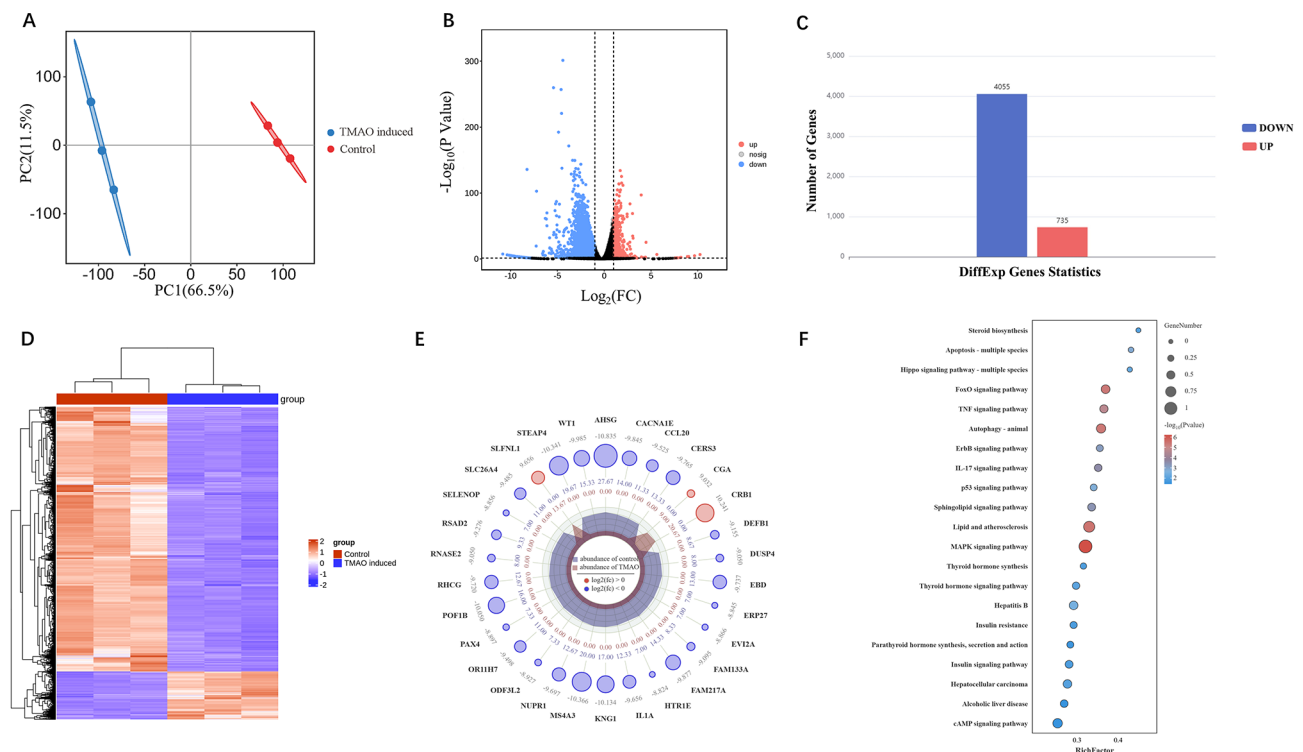


**Fig. 3** Transcriptomic analysis reveals the impact of 400 μmol/L TMAO treatment on gene expression in bovine hepatic cells. (**A**) PCA plot demonstrates the overall expression pattern differences between control and TMAO-treated bovine hepatic cell samples. (**B**) A volcano plot depicts the relationship between the significance of differentially expressed genes (-log10(p-value)) and the magnitude of expression change (log2 fold change), with red points indicating significantly upregulated genes, blue points denoting significantly downregulated genes, and black points representing genes with no significant difference. (**C**) A bar chart of the number of differentially expressed genes illustrates the count of significantly upregulated and downregulated genes in the TMAO-treated group. (**D**) A heatmap of differentially expressed genes displays the genes with significant expression differences between the control and TMAO-treated groups. The color gradient from blue (low expression) to red (high expression) indicates the level of expression change. (**E**) A radar chart shows the functional distribution of the top 20 genes with the most significant expression changes. (**F**) A KEGG enrichment analysis plot presents the enrichment of differentially expressed genes in metabolic pathways, with the size indicating the number of genes and the color intensity reflecting the level of enrichment significance

differentially expressed genes (Supplementary Table S2, FDR<0.05), with 735 genes upregulated and 4055 genes downregulated (Fig. 3B and C). A heatmap was generated through cluster analysis of the differentially expressed genes, demonstrating good reproducibility within groups

and clear differences between groups (Fig. 3D). This indicates that TMAO treatment of bovine hepatic cells can significantly alter the gene expression levels in liver cells. To present the significant differences more visually between the two comparison groups, a radar chart was

created, detailing the expression patterns of the top 20 differentially expressed genes (Fig. 3E).

The KEGG pathway enrichment analysis of differentially expressed genes revealed several key pathways related to metabolism, inflammation and oxidative stress, and signal transduction. The analysis indicated that pathways related to metabolism were mainly concentrated in steroid biosynthesis, and thyroid hormone synthesis. Pathways related to inflammation and oxidative stress were primarily enriched in lipid and atherosclerosis, hepatitis B pathways ($P<0.05$, Fig. 3F). As for signal transduction, the involved pathways included insulin resistance, MAPK signaling pathway, thyroid hormone signaling pathway, and insulin signaling pathway, which are critical pathways.

## Identification and comparison of differentially abundant proteins

To elucidate the mechanism of action of TMAO in bovine hepatic cell lipid metabolism, this study employed a LFQ proteomics approach to identify proteins within

bovine hepatic cells. As shown in Fig. 4A, the identified peptide lengths were primarily concentrated above 10 amino acids (aa), indicating high data quality and providing a reliable foundation for subsequent analyses. PCA scatter plots revealed a clear separation between the TMAO-treated group and the control group along the first principal component (PC1), suggesting that TMAO treatment significantly altered the overall protein expression pattern in bovine hepatic cells (see Fig. 4B). Further differential expression analysis yielded a total of 397 significantly different proteins (Supplementary Table S3, $P<0.05$), with 232 proteins upregulated and 165 downregulated (Fig. 4C and D). Cluster heatmap analysis visually displayed the expression differences of these proteins between different treatment groups (Fig. 4E).

The KEGG enrichment results of differentially abundant proteins indicated that metabolic pathways were mainly enriched in metabolic pathways, central carbon metabolism in cancer, inositol phosphate metabolism, and carbohydrate digestion and absorption. Pathways related to inflammation and oxidative stress
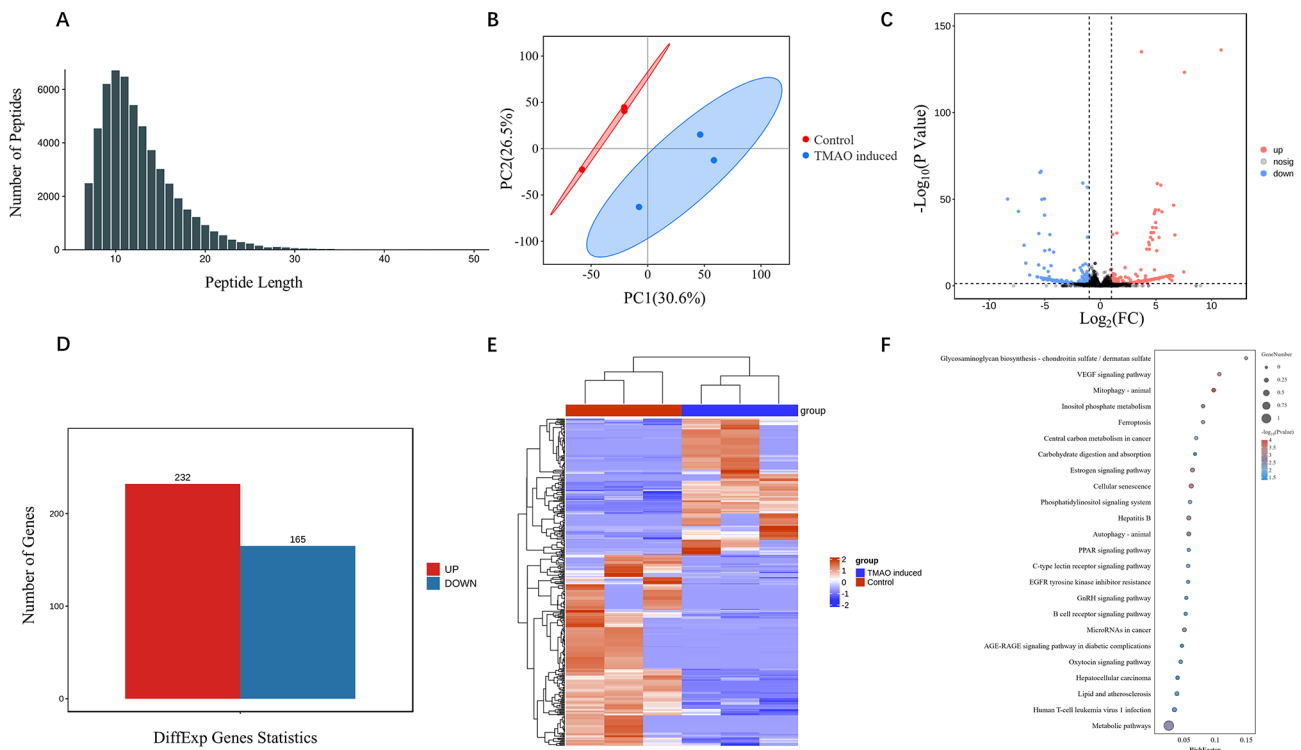


**Fig. 4** Overview of proteomic analysis results depicting the impact of 400 µmol/L TMAO treatment on protein expression in bovine hepatic cells. (**A**) The peptide length distribution chart ensures the quality of protein identification by reflecting the distribution of identified peptide lengths. (**B**) PCA plots demonstrate the overall differences in protein expression patterns between control and TMAO-treated bovine hepatic cell samples. (**C**) Volcano plots reveal the relationship between the significance of differentially expressed proteins and the fold change in expression, with red points representing significantly upregulated proteins, blue points indicating significantly downregulated proteins, and black points denoting proteins with no significant difference. (**D**) A bar chart of the number of significantly differentially abundant proteins provides a clear visualization of the counts of proteins that are significantly upregulated and downregulated in the TMAO-treated group. (**E**) A heatmap of differentially expressed proteins shows those with the most significant expression differences between the control and TMAO-treated groups, with a color gradient from blue to red indicating decreasing and increasing protein expression levels, respectively. (**F**) A KEGG enrichment analysis plot reveals the enrichment of differentially expressed proteins in metabolic pathways, with the size of the circles representing the number of proteins and the color intensity indicating the level of enrichment significance

Li *et al. BMC Genomics*          (2025) 26:10

Page 8 of 17

were primarily enriched in lipid and atherosclerosis and hepatitis B pathways ($P<0.05$, Fig. 4F). In contrast, signal transduction-related pathways included the AGE-RAGE signaling pathway in diabetic complications and the phosphatidylinositol signaling system, among other critical pathways.

## Identification and comparison of differential metabolites

To delve into the metabolic mechanisms of TMAO's effects on bovine hepatic cells, this study utilized an untargeted metabolomics approach to analyze the metabolites of the experimental and control groups. The results of the PCA revealed significant differences in the metabolic profiles between the two groups, with good biological reproducibility within each group ( Fig. 5A). Moreover, the OPLS-DA score plots indicated a distinct separation between the two sample groups under both positive and negative ion modes. The validity of the OPLS-DA models was confirmed by 200 permutation tests, yielding model quality parameters ($R2Y=0.998$ and $Q2=0.952$ for positive ion mode; $R2Y=0.992$ and $Q2=0.931$ for negative ion mode) that demonstrated high stability and the absence of overfitting ( Fig. 5B and C). Differential analysis identified a total of 137 significantly altered metabolites (Fig. 5D and E), with 89 metabolites significantly upregulated (67 in positive ion mode and 22

in negative ion mode, Supplementary Table S4) and 48 significantly downregulated (34 in positive ion mode and 14 in negative ion mode). These differential metabolites were subsequently used for cluster analysis (Fig. 6A).

KEGG pathway enrichment analysis was conducted on the 137 differential metabolites to investigate the biological pathways potentially affected by TMAO in bovine hepatic cells. The results indicated that the pathways related to metabolism were predominantly concentrated in beta-alanine metabolism, central carbon metabolism in cancer, and the metabolism of glycine, serine, and threonine, as well as oxidative phosphorylation. Pathways associated with inflammation and oxidative stress were mainly enriched in type II diabetes and neurodegenerative diseases - multiple diseases ($P<0.05$, Fig. 6B). Signal transduction-related pathways included key pathways such as the AMPK signaling pathway and insulin secretion.

## Integrated multi-omics data analysis

By integrating transcriptomic, proteomic, and metabolomic data, and analyzing pathways significantly enriched ($P<0.05$), we constructed a comprehensive regulatory network for lipid metabolism. As shown in Fig. 7, this network reveals the multifaceted impact of TMAO on lipid metabolism in bovine hepatic cells, demonstrating
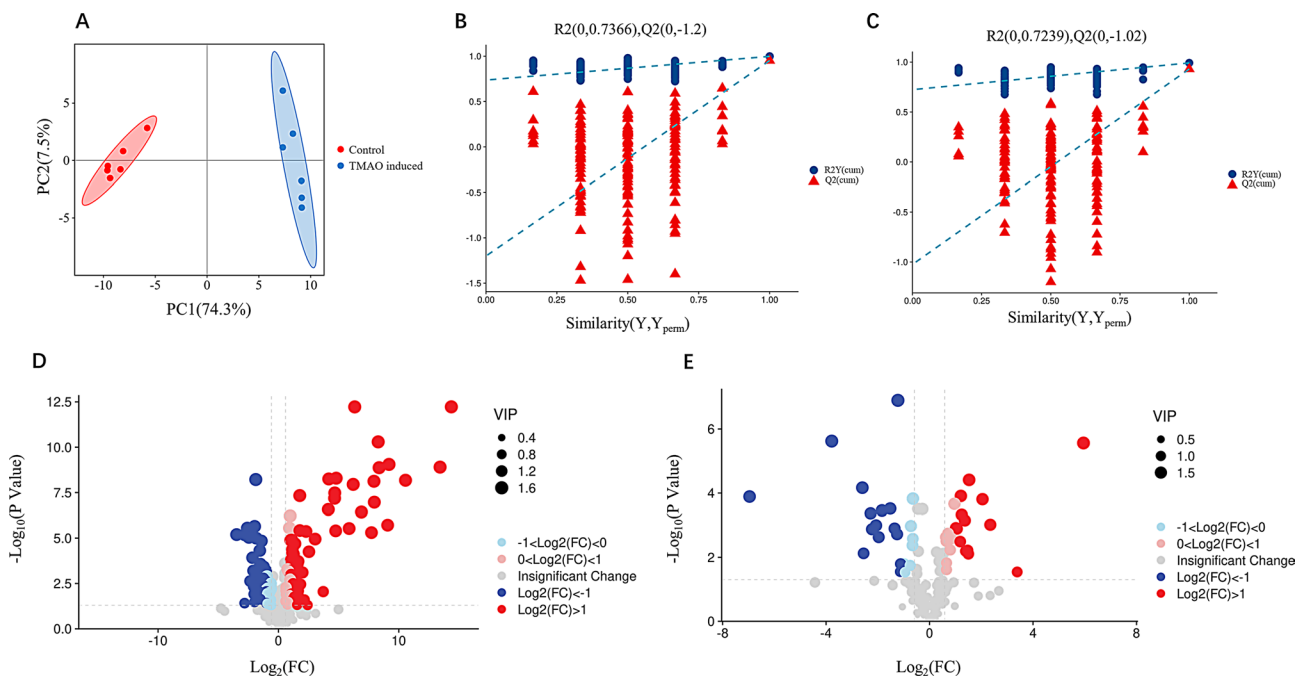


**Fig. 5** Analytical results of the impact of 400 µmol/L TMAO treatment on the metabolic spectrum of bovine hepatic cells. (**A**) PCA plots illustrate the overall distribution and variability of the metabolites at the metabolic level between the control and TMAO-treated groups. (**B** and **C**) The quality parameters of the orthogonal partial least squares discriminant analysis (OPLS-DA) scoring models under positive and negative ion modes provide information on the model fitting quality and predictive capability, including $R^2$ and $Q^2$ values. (**D** and **E**) Volcano plots under positive and negative ion modes depict the relationship between the significance of metabolites (-log10(p-value)) and fold changes (log2 fold change), with red and blue points indicating significantly upregulated and downregulated metabolites, respectively
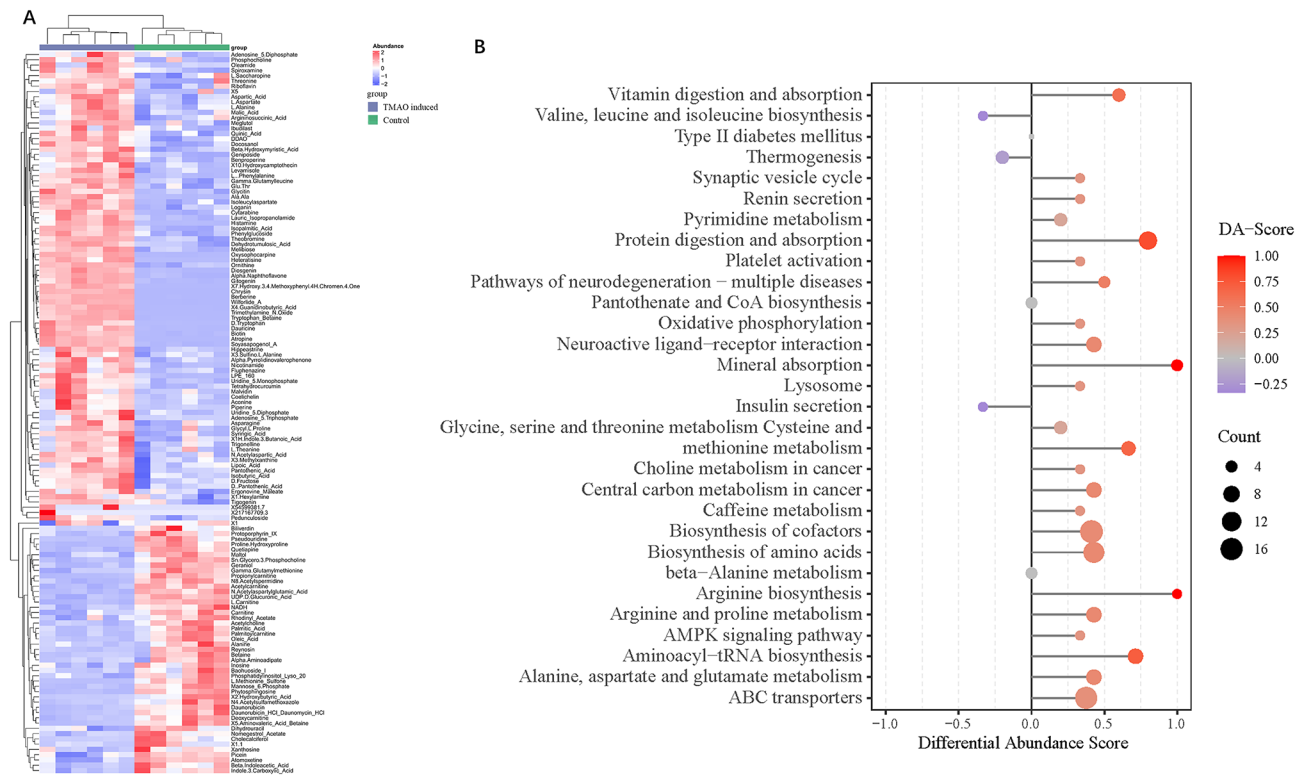
**Fig. 6** Characterization of Differential Metabolites. (**A**) A heatmap of differential metabolites illustrates the variations in metabolite expression levels between TMAO-treated and control bovine hepatic cells. The color gradient in the heatmap transitions from blue (low expression) to red (high expression), indicating changes in metabolite abundance and representing the relative expression levels of various metabolites across the samples. (**B**) The Differential Abundance (DA) score results display the overall trend of metabolite changes in pathways relative to the control group. The x-axis represents the collective trend changes of all metabolites within a metabolic pathway, while the y-axis corresponds to the pathways themselves. The size of the circles indicates the number of metabolites annotated within that pathway, and the color transitions from blue to red represent DA scores ranging from − 1 to 1. A DA score of -1 implies that the abundance of all metabolites in that pathway has decreased, whereas a DA score of 1 indicates an increase in abundance of all metabolites within the pathway. The closer the DA score is to 1 or -1, the more the overall expression in the pathway tends toward upregulation or downregulation, respectively

that TMAO treatment significantly affects signaling pathways, lipid metabolism pathways, and inflammation-related pathways. To further explore the interactions between key genes, proteins, and metabolites related to lipid metabolism in bovine hepatic cells after TMAO treatment, we conducted Pearson correlation analysis (Supplementary Figs. 1, 2, and 3) and constructed a correlation network diagram (Fig. 8). The analysis revealed that NADH has a highly significant correlation ($P<0.01$) with most key genes and proteins, which are significantly enriched in signaling pathways, lipid metabolism pathways, and inflammation-related pathways ($P<0.05$), suggesting that they may play important roles in TMAO-mediated lipid metabolism regulation. Finally, by integrating multi-omics data analysis, we revealed the potential mechanisms of TMAO's impact on lipid metabolism in bovine hepatic cells. As illustrated in Fig. 9, the schematic diagram details the interplay between the TMAO-mediated AMPK signaling pathway and oxidative phosphorylation pathway, revealing how they cooperatively regulate the lipid metabolism

process. Specifically, NADH, the primary electron donor in aerobic respiration, exhibited a significant downregulation, leading to reduced efficiency of the electron transport chain, which affects the synthesis of ATP and ADP. Notably, our data show a significant increase in ATP levels following TMAO treatment, which may be attributable to metabolic regulation induced by TMAO. With the significant upregulation of ATP levels, the ratio of ADP to ATP decreases, placing the bovine hepatic cells in a high-energy state, which further inhibits the AMPK signaling pathway. AMPK is an intracellular energy sensor, typically activated during energy scarcity to promote energy production and inhibit energy-consuming pathways. Therefore, we hypothesize that under the influence of TMAO, the suppression of the AMPK signaling pathway activates lipid synthesis pathways, thereby promoting lipid accumulation.

**Quantitative real time-PCR validation**

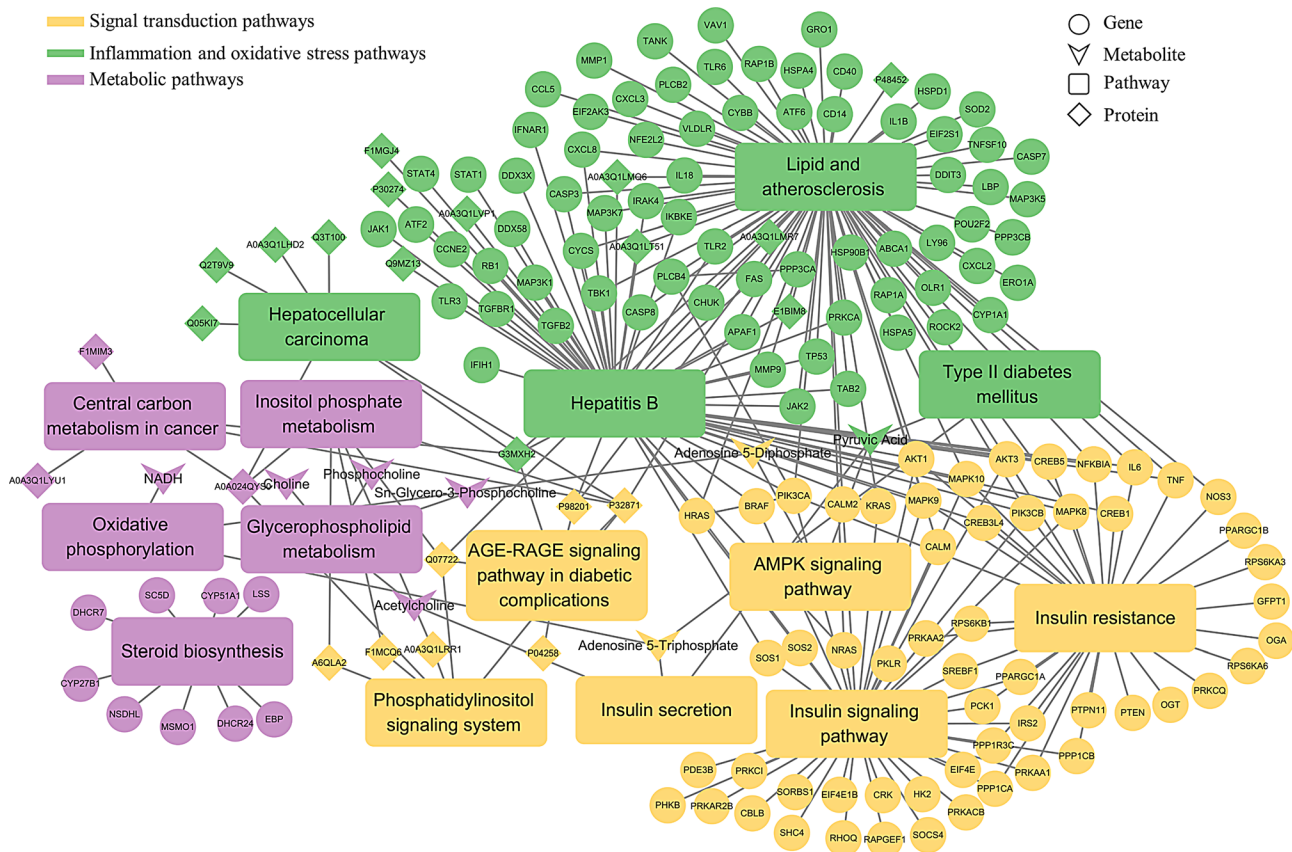To verify the reliability of our transcriptomic data, we performed qRT-PCR validation. Nine differentially

**Fig. 7** Lipid Metabolism Regulatory Network Revealed by Multi-Omics Data Analysis. The figure presents a lipid metabolism regulatory network constructed through the integration of proteomic, transcriptomic, and metabolomic data. The nodes in the network diagram represent categories, including genes, proteins, metabolites, and pathways, while edges denote the interactions or regulatory relationships between these molecules. The color of the nodes indicates the biological functions in which the molecules are involved

expressed genes associated with lipid metabolism pathways were randomly selected for this purpose, including Acyl-CoA Synthetase Long Chain Family Member 3 (*ACSL3*, $\log_2$FC=-1.717), Acetyl-CoA Carboxylase Alpha (*ACACA*, $\log_2$FC=1.15), Carnitine Palmitoyltransferase 2 (*CPT2*, $\log_2$FC=1.03), CREB Binding Protein (*CREBBP*, $\log_2$FC=1.26), Cytochrome P450 Family 1 Subfamily A Member 1 (*CYP1A1*, $\log_2$FC=2.71), Low Density Lipoprotein Receptor (*LDLR*, $\log_2$FC=1.04), Lipin 2 (*LPIN2*, $\log_2$FC=1.01), Sterol Carrier Protein 2 (*SCP2*, $\log_2$FC=-1.95), and Sterol Regulatory Element Binding Transcription Factor 1 (*SREBF1*, $\log_2$FC=1.85). The results demonstrated that the expression trends of the genes verified by qRT-PCR were generally consistent with the transcriptome sequencing results (Supplementary Fig. 4), indicating that the experimental transcriptomic data are stable and reliable. To further investigate the impact of TMAO on the AMPK signaling pathway, we examined three key genes within this pathway: *MO25*, *AMPK*, and *SREBF1*. The experimental outcomes revealed that under the influence of TMAO, the expression of the *MO25* gene was significantly downregulated

(Fig. 10B, *P*<0.01), and the expression of the *AMPK* gene was notably decreased (Fig. 10C, *P*<0.05). These findings suggest that TMAO may inhibit the core components of the AMPK signaling pathway, thereby affecting its activity and function. Concurrently, we observed a significant increase in the expression of the critical lipid metabolism regulatory transcription factor gene *SREBF1* in the TMAO-treated group (Fig. 10A, *P*<0.05). This observation aligns with our hypothesis that TMAO promotes the expression of genes related to lipid synthesis by inhibiting the AMPK signaling pathway. These quantitative validation results provide robust support for our multi-omics analysis and further confirm the regulatory effects of TMAO on the AMPK signaling pathway.

## Discussion

In contemporary animal husbandry, the health and productive efficiency of dairy cows are intricately linked to the equilibrium of their lipid metabolism. Dysregulation of lipid metabolism not only poses a threat to the quality and yield of dairy products but may also precipitate metabolic disorders such as fatty liver and ketosis. Therefore,
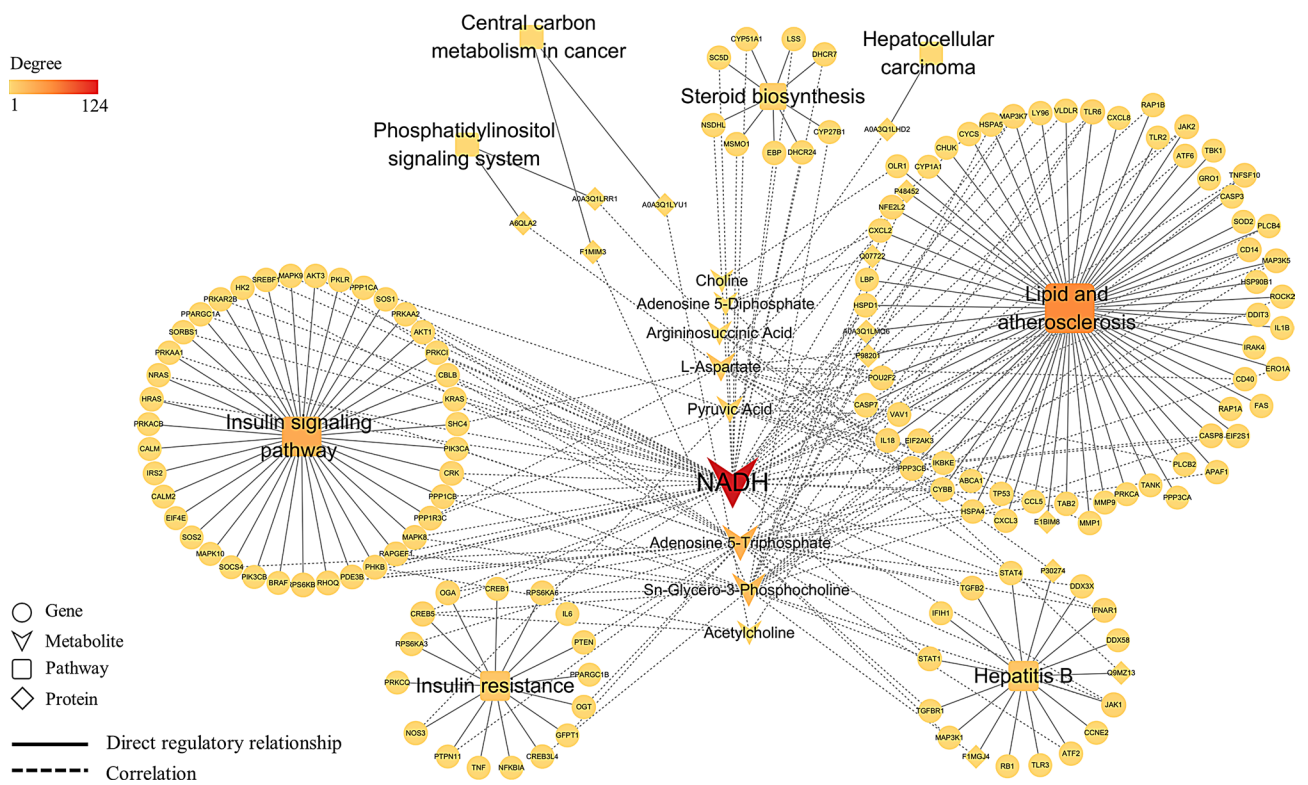
**Fig. 8** Pearson Correlation Network of Lipid Metabolism-Related Molecules in Bovine Hepatic Cells Following TMAO Treatment. This figure, based on Pearson correlation analysis results, depicts the interaction network among key genes, proteins, and metabolites in bovine hepatic cells after TMAO treatment. The types of nodes in the network diagram represent categories, including genes, proteins, metabolites, and pathways. Edges represent different regulatory relationships, with dashed lines indicating highly significant correlations ($P < 0.01$) and solid lines representing direct regulatory relationships. The color and size of the nodes reflect the relative importance of the molecules within the network

a profound understanding of the intrinsic regulatory mechanisms governing bovine lipid metabolism is of paramount importance for enhancing dairy cattle welfare and milk production levels. TMAO a ubiquitous nutritional metabolite in humans and animals, has garnered extensive attention for its impact on lipid metabolism [41–44]. However, the specific role of TMAO in bovine lipid metabolism remains incompletely elucidated. This study is dedicated to uncovering the regulatory role of TMAO in lipid metabolism within bovine hepatic cells. Adopting a systems biology approach, we considered the interactive network between molecules and pathways. Initially, we determined the optimal concentration of TMAO based on hepatic function indicators and TG content in bovine hepatic cells. Through multi-omics sequencing analysis, we elucidated that TMAO significantly modulates the expression of a suite of key genes, proteins, and metabolites related to lipid metabolism. These components play pivotal roles in signal transduction pathways, lipid metabolism pathways, and inflammatory response pathways. Notably, in our constructed lipid metabolism regulatory network, NADH occupies a central position in metabolic regulation. Ultimately, we developed a dynamic interaction model between the

TMAO-mediated AMPK signaling pathway and oxidative phosphorylation pathway, thereby revealing their synergistic roles in lipid metabolism regulation. Our research provides new insights into how TMAO affects lipid metabolism in bovine hepatic cells, findings that may have significant implications for improving the health and productive performance of dairy cattle.

In dairy cows, especially high-yielding ones, fatty liver is primarily related to inadequate postpartum nutritional intake, a condition exacerbated by the significant increase in energy demands after calving, leading to massive breakdown of body fat and ultimately promoting lipid deposition in liver cells [45, 46]. The development mechanism of fatty liver in dairy cows is similar to that of human NAFLD, involving an imbalance in lipid metabolism pathways. In dairy cows, the formation of fatty liver is closely linked to various metabolic processes such as fatty acid synthesis, oxidation, and export. The high energy demands postpartum trigger the release of a large amount of fatty acids from adipose tissue, but the liver's capacity for fatty acid oxidation is limited, unable to effectively process these excess fatty acids, resulting in lipid accumulation within liver cells [47–50]. In exploring the mechanisms of lipid metabolism disorder, the AMPK
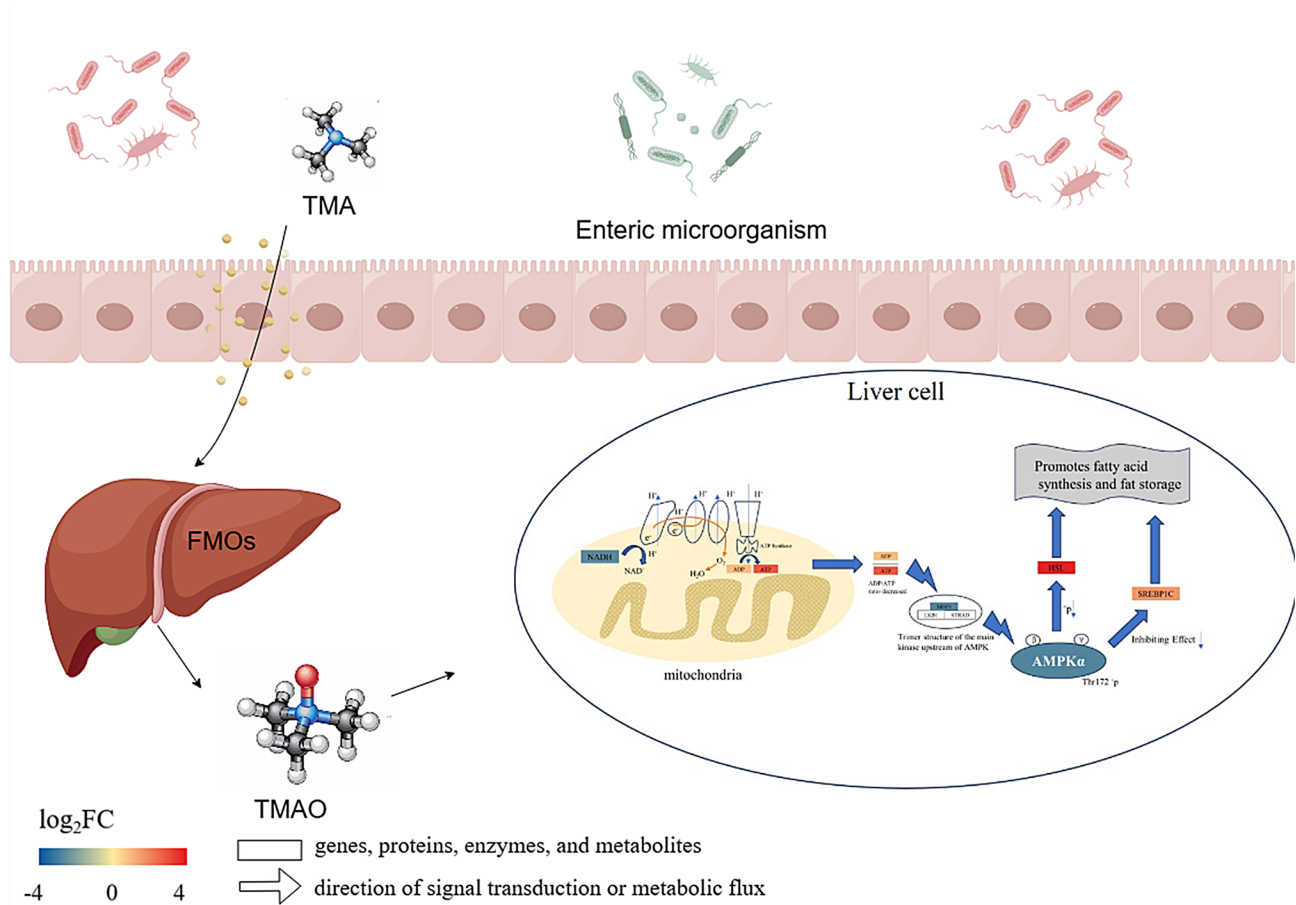
**Fig. 9** Schematic Model of TMAO-Mediated Lipid Metabolism Regulatory Mechanism. This figure provides a detailed illustration of the interplay between the AMPK signaling pathway and the oxidative phosphorylation pathway in bovine hepatic cells following TMAO treatment, as well as the potential mechanisms by which they cooperatively regulate lipid metabolism. Rectangles in the diagram represent genes, proteins, enzymes, and metabolites, with arrows indicating the direction of signal transduction or metabolic flux. Different colors denote regulatory relationships, with red indicating upregulation and blue indicating downregulation
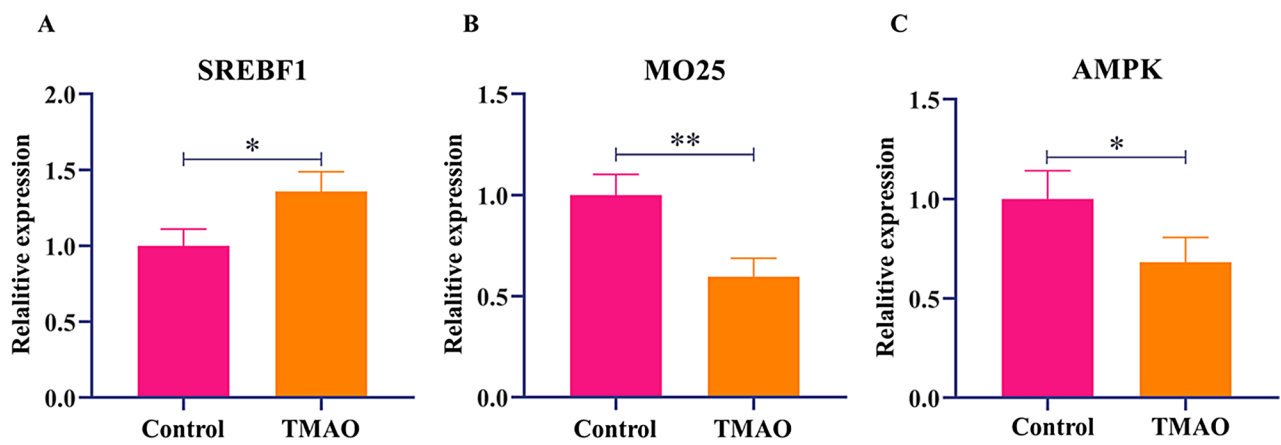


•SREBF1 (Sterol Regulatory Element Binding Transcription Factor 1)
•MO25 (Calcium Binding Protein 39, CAB39)
•AMPK (Adenosine Monophosphate-Activated Protein Kinase)

**Fig. 10** qRT-PCR validation of key genes in the AMPK pathway. (**A**) Relative expression level of the *SREBF1* gene. (**B**) Relative expression level of the *MO25* gene. (**C**) Relative expression level of the *AMPK* gene. * indicates $P < 0.05$, ** indicates $P < 0.01$

Li *et al. BMC Genomics*        (2025) 26:10

Page 13 of 17

signaling pathway is considered to play a significant role. Studies by Fang et al. have underscored the role of AMPK in improving dysregulated lipid metabolism, indicating that the activation of the AMPK signaling axis is crucial for preventing and mitigating liver damage, and that AMPK activation can alleviate liver damage caused by alcohol or insulin resistance [51]. while Yan et al. found that Schisandrin B could induce autophagy through the AMPK/mTOR signaling pathway, thereby alleviating liver steatosis and promoting fatty acid oxidation [52]. We examined three key genes within this pathway: *MO25*, *AMPK*, and *SREBF1*. The experimental outcomes revealed that under the influence of TMAO, the expression of the *MO25* gene was significantly downregulated (Fig. 10B, $P < 0.01$), and the expression of the *AMPK* gene was notably decreased (Fig. 10C, $P < 0.05$). These findings suggest that TMAO may inhibit the core components of the AMPK signaling pathway, thereby affecting its activity and function. Concurrently, we observed a significant increase in the expression of the critical lipid metabolism regulatory transcription factor gene *SREBF1* in the TMAO-treated group (Fig. 10A, $P < 0.05$). Our study results indicate that TMAO may regulate fatty acid synthesis and oxidation by affecting the AMPK signaling pathway, consistent with AMPK's core regulatory role in energy metabolism. Moreover, the reduction in AMPK activity is closely related to the development of NAFLD, aligning with our observation of TMAO's inhibitory effect on the AMPK signaling pathway, providing further evidence of TMAO's potential role in regulating bovine lipid metabolism. The occurrence of postpartum insulin resistance in dairy cows is also related to the formation of fatty liver. The role of insulin resistance in the formation of fatty liver in dairy cows may be realized through multiple molecular mechanisms. Firstly, insulin resistance reduces the responsiveness of liver cells to insulin, leading to a decrease in insulin-mediated fatty acid synthesis and an obstruction in the activation of fatty acid oxidation pathways, thereby promoting lipid accumulation in the liver [53–55].Sudies by Hosokawa et al. have revealed mechanisms by which insulin resistance in adipose tissue and a high-fat diet (GAN diet) may exacerbate liver damage through promoting inflammation and fibrosis [56]. These findings corroborate our KEGG pathway enrichment analysis results. Through transcriptomic and proteomic analyses, we detected significant expression changes in several key molecules within the insulin signaling pathway. For example, the Ras gene was significantly upregulated ($Log_2FC = 1.2$), with a corresponding increase in protein levels ($Log_2FC = 1.6$). Similarly, the GRF2 gene expression was upregulated ($Log_2FC = 1.1$), and its protein level markedly increased ($Log_2FC = 5.3$). Conversely, both the GK gene and its protein levels were downregulated ($Log_2FC = -1.1$, protein

$Log_2FC = -1.2$). These results indicate that the upregulation of mRNA levels generally corresponds to an increase in protein levels. Moreover, the consistent significant changes observed at both the transcriptional and protein levels for key metabolic enzymes underscore the coordinated regulation between transcription and translation. Furthermore, the postpartum inflammatory and oxidative stress states in dairy cows may also exacerbate lipid deposition in the liver, further impairing liver function. Research by Zhang et al. suggests that liver inflammation and oxidative stress are often associated with the occurrence and progression of chronic liver disease (CLD). In this process, key molecular signaling pathways such as AMPK and peroxisome proliferator-activated receptors (PPARs) are closely related to the pathological mechanisms of CLD [57]. Studies by Qiu et al. found that Panax japonicus (PJ) could upregulate the AMPK-ACC/ PPARα axis, reduce liver lipid deposition, and decrease the expression of IL-6 and TNF-α, indicating a reduction in lipid peroxidation in the liver [58]. Our KEGG enrichment analysis results also significantly enriched pathways closely related to liver inflammation, such as hepatitis B, type 2 diabetes, and hepatocellular carcinoma, further indicating that the development of fatty liver is not merely a single metabolic disorder event but a complex pathological state involving multiple biological processes and signaling pathways. The dysregulation of these pathways may reflect the internal inflammation and oxidative stress response triggered by increased postpartum metabolic stress. Accordingly, we speculate that inflammatory and oxidative stress pathways are also key factors driving the development of fatty liver. This finding further emphasizes the importance of maintaining anti-inflammatory and antioxidative balance in the liver during the critical postpartum period in dairy cows. In summary, the formation of fatty liver in dairy cows is a complex multi-step process involving the AMPK signaling pathway, insulin signal transduction, and other links. These include reduced downstream signal transduction efficiency of insulin receptors, regulatory imbalances in key metabolic pathways, and the activation of inflammation and fibrosis processes. In-depth research on these pathways is crucial for developing effective prevention and treatment strategies, not only helping to improve the health and welfare of dairy cows but also contributing to the overall economic efficiency of the dairy industry.

TMA is the precursor of TMAO, primarily originates from foods rich in choline, phosphatidylcholine, and L-carnitine, such as red meat, fish, eggs, and dairy products [59]. Under the action of gut microbiota, these substances are broken down into TMA, which is subsequently absorbed into the bloodstream through the intestinal wall. In the liver, TMA is oxidized to TMAO by the enzyme flavin-containing monooxygenase 3 (FMO3) [60,

61]. Research has shown that TMAO interferes with the AMP-activated protein kinase (AMPK) signaling pathway, affecting the synthesis and breakdown of fatty acids, leading to lipid accumulation in the liver and non-alcoholic fatty liver disease (NAFLD) [62, 63]. Additionally, TMAO enhances inflammatory responses and oxidative stress, promoting the development of atherosclerosis. It is also associated with insulin resistance and type 2 diabetes, potentially by promoting inflammation and lipid metabolic disorders that interfere with insulin signaling [14]. Our study reveals significant alterations in the levels of ATP, NADH, and ADP following TMAO treatment. Specifically, NADH levels were significantly downregulated ($Log_2FC = -2.07$), ADP levels were significantly upregulated ($Log_2FC=0.66$), and ATP levels showed a substantial increase ($Log_2FC=3.38$). These metabolic changes may be attributed to a redistribution of cellular energy metabolism, with TMAO potentially triggering other metabolic pathways such as glycolysis to compensate for the increased ATP demand [64, 65].AMPK, a cellular energy sensor, is typically activated when cellular energy levels (ATP) are low to enhance energy production and inhibit energy consumption [66, 67]. However, in the context of significantly elevated ATP levels ($Log_2FC=3.38$), the AMPK pathway is inhibited. Our data indicate a significant downregulation in the expression of MO25 and AMPK. MO25, a critical component of the AMPK complex, interacts with the AMPK α-subunit and liver kinase B1 (LKB1) and is essential for the activation and stability of AMPK. The downregulation of MO25 compromises the stability and activity of the AMPK complex, subsequently inhibiting AMPK activation and weakening its regulatory role in energy metabolism [68].The inhibition of AMPK activity further affects downstream metabolic pathways, including the expression of hormone-sensitive lipase (HSL) and *SREBP1c*. Normally, AMPK activation suppresses the activities of HSL and *SREBP1c*, reducing lipid catabolism and anabolism [69–72]. However, when AMPK is inhibited, we observed a significant upregulation in HSL and SREBP1c expression, with $Log_2FC$ values of 3.72 and 1.8, respectively. This upregulation indicates increased fatty acid release and synthesis, leading to lipid metabolic imbalance. This lipid metabolic imbalance may cause excessive lipid accumulation in the liver. If these fatty acids are not efficiently utilized, such as through mitochondrial β-oxidation, they may be re-esterified into TG and stored in the liver. This process contributes to the development of hepatic steatosis and increases the risk of metabolic disorders such as non-alcoholic fatty liver disease (NAFLD) and cardiovascular diseases [47, 73].In conclusion, our research reveals that TMAO, by influencing the gut-liver axis, alters the levels of key metabolites such as ATP, NADH, and ADP, thereby inhibiting the AMPK signaling pathway. The inhibition

of the AMPK pathway further affects HSL and SREBP1c expression, leading to lipid metabolic imbalance and increased hepatic lipid accumulation. These findings are crucial for understanding the role of the gut-liver axis in TMAO-induced lipid metabolic disorders and their potential implications in NAFLD.

In this study, we explored the implications of TMAO on the development of NAFLD in cattle. Although direct research on TMAO in cattle remains sparse, findings from human studies provide valuable insights. This cross-species reference is supported by the similar roles TMAO plays in lipid metabolism and inflammation in both humans and potentially cattle. However, it is crucial to acknowledge the limitations of this extrapolation. Physiological differences between species can impact the direct applicability of human findings to cattle. For instance, metabolic pathways and gut microbiota compositions are known to vary, which may influence TMAO's effects. Furthermore, the criteria and thresholds used in our correlation analysis (e.g., $log_2FC>1$, VIP≥1, and FC>1.5 or FC<0.667) were chosen to ensure a focus on significant changes, potentially impacting the broader interpretation of our results. While these thresholds help filter out less significant data, they may also exclude subtle yet important interactions. These limitations highlight the importance of cautious interpretation of our findings and suggest a need for further investigation, possibly incorporating more flexible criteria or additional complementary analyses. Future research should focus on experimental validation of these findings in cattle to confirm the hypothesized pathways and regulatory mechanisms derived from human studies and our current analysis.

In summary, we have discovered that TMAO exerts a significant impact on lipid metabolism in bovine liver cells, further elucidating the potential molecular mechanisms of TMAO in the metabolic regulation of dairy cows. Nonetheless, the current study relies on data obtained from in vitro cell models, which limits our ability to apply these findings directly to practical dairy production. Therefore, to validate our discoveries and ensure their biological significance, it is imperative to conduct subsequent research under in vivo conditions. Future work should focus on the actual role of TMAO in lipid metabolism within bovine liver cells in vivo, and extend to its impact on the overall metabolic processes of the animals. Moreover, exploring the potential applications of TMAO production mechanisms in enhancing dairy production efficiency and health status holds significant research value. For instance, by adjusting feed formulations to reduce TMAO production, we could alleviate the metabolic burden on the liver, thereby improving dairy yield and quality. Through in-depth research, we aim not only to deepen our understanding of the role of TMAO in bovine lipid metabolism but also to provide a

Li *et al. BMC Genomics*          (2025) 26:10

Page 15 of 17

solid scientific basis for the nutritional management and health maintenance of dairy cows.

## Conclusion

In this study, a bovine hepatic steatosis cell model was established, and a systems biology approach was employed to integrate transcriptomic, proteomic, and metabolomic data, thereby comprehensively dissecting the impact of TMAO on lipid metabolism in bovine liver cells. Through in-depth bioinformatics analysis, we unveiled the mechanisms of action of TMAO in bovine liver cells. Specifically, this research meticulously elucidated the mechanism by which the interaction between the TMAO-mediated AMPK signaling pathway and the oxidative phosphorylation pathway promotes hepatic lipid deposition. The findings of this study offer new insights into the prevention and treatment of fatty liver in dairy cows. By conducting such multidimensional research, we can better understand the complexity of metabolic diseases in dairy cows, contributing to the sustainable development of the dairy industry.

## Supplementary Information

The online version contains supplementary material available at https://doi.or g/10.1186/s12864-024-11067-7.

Supplementary Material 1

Supplementary Material 2

### Data availability
The raw sequencing data have been uploaded to the NCBI database under BioProject ID PRJNA1028383. For further information, please feel free to contact the corresponding author.

## Declarations

### Ethics approval and consent to participate
The animal study was approved by the Institutional Animal Care and Use Committee of Ningxia University (NXUC20220220). The study was conducted in accordance with the local legislation and institutional requirements.

### Consent for publication
Not applicable.

### Competing interests
The authors declare no competing interests.

## References
1. Shahryari M, Keller S, Meierhofer D, Wallach I, Safraou Y, Guo J, Marticorena Garcia SR, Braun J, Makowski MR, Sack I, et al. On the relationship between metabolic capacities and in vivo viscoelastic properties of the liver. Front Bioeng Biotechnol. 2022;10:1042711.
2. Hyun J, Han J, Lee C, Yoon M, Jung Y. Pathophysiological aspects of Alcohol Metabolism in the liver. Int J Mol Sci 2021, 22(11).
3. Alannan M, Fayyad-Kazan H, Trézéguet V, Merched A. Targeting lipid metabolism in Liver Cancer. Biochemistry. 2020;59(41):3951–64.
4. Badmus OO, Hillhouse SA, Anderson CD, Hinds TD, Stec DE. Molecular mechanisms of metabolic associated fatty liver disease (MAFLD): functional analysis of lipid metabolism pathways. Clin Sci. 2022;136(18):1347–66.
5. Bian X, Liu R, Meng Y, Xing D, Xu D, Lu Z. Lipid metabolism and cancer. J Exp Med 2021, 218(1).
6. Johnson AA, Stolzing A. The role of lipid metabolism in aging, lifespan regulation, and age-related disease. Aging Cell. 2019;18(6):e13048.
7. Ghaffari MH, Sanz-Fernandez MV, Sadri H, Sauerwein H, Schuchardt S, Martín-Tereso J, Daniel JB. Longitudinal characterization of the metabolome of dairy cows transitioning from one lactation to the next one: investigations in the liver. J Dairy Sci 2024.
8. Martens H. [The lipidosis in the liver of the dairy cow: part 2 genetic predisposition and prophylaxis]. Tierarztl Prax Ausg G Grosstiere Nutztiere. 2023;51(5):305–13.
9. Wang J, Zhu X, She G, Kong Y, Guo Y, Wang Z, Liu G, Zhao B. Serum hepatokines in dairy cows: periparturient variation and changes in energy-related metabolic disorders. BMC Vet Res. 2018;14(1):236.
10. Zhang F, Nan X, Wang H, Zhao Y, Guo Y, Xiong B. Effects of propylene glycol on negative energy balance of Postpartum dairy cows. Anim (Basel) 2020, 10(9).
11. Xu W, van Knegsel A, Saccenti E, van Hoeij R, Kemp B, Vervoort J. Metabolomics of milk reflects a negative energy balance in cows. J Proteome Res. 2020;19(8):2942–9.
12. Schoeler M, Caesar R. Dietary lipids, gut microbiota and lipid metabolism. Rev Endocr Metab Disord. 2019;20(4):461–72.
13. Gatarek P, Kaluzna-Czaplinska J. Trimethylamine N-oxide (TMAO) in human health. Excli j. 2021;20:301–19.
14. Thomas MS, Fernandez ML. Trimethylamine N-Oxide (TMAO), Diet and Cardiovascular Disease. Curr Atheroscler Rep. 2021;23(4):12.
15. Din AU, Hassan A, Zhu Y, Yin T, Gregersen H, Wang G. Amelioration of TMAO through probiotics and its potential role in atherosclerosis. Appl Microbiol Biotechnol. 2019;103(23–24):9217–28.
16. Lombardo M, Aulisa G, Marcon D, Rizzo G. The influence of animal- or plant-based diets on blood and urine Trimethylamine-N-Oxide (TMAO) levels in humans. Curr Nutr Rep. 2022;11(1):56–68.
17. Saaoud F, Liu L, Xu K, Cueto R, Shao Y, Lu Y, Sun Y, Snyder NW, Wu S, Yang L et al. Aorta- and liver-generated TMAO enhances trained immunity for increased inflammation via ER stress/mitochondrial ROS/glycolysis pathways. JCI Insight 2023, 8(1).
18. Nian F, Zhu C, Jin N, Xia Q, Wu L, Lu X. Gut microbiota metabolite TMAO promoted lipid deposition and fibrosis process via KRT17 in fatty liver cells in vitro. Biochem Biophys Res Commun. 2023;669:134–42.
19. Li Y, Zhang L, Ren P, Yang Y, Li S, Qin X, Zhang M, Zhou M, Liu W. Qing-Xue-Xiao-Zhi formula attenuates atherosclerosis by inhibiting macrophage lipid accumulation and inflammatory response via TLR4/MyD88/NF-κB pathway regulation. Phytomedicine. 2021;93:153812.
20. Vourakis M, Mayer G, Rousseau G. The role of gut microbiota on cholesterol metabolism in atherosclerosis. Int J Mol Sci 2021, 22(15).
21. Fei'erdun T, Zhang W, Yilihamujiang K, Zhang M, Wang M. [Correlation between plasma trimethylamine N-Oxide and lipid levels in hyperlipidemic patients]. Sichuan Da Xue Xue Bao Yi Xue Ban. 2023;54(5):1030–4.

22. Tan X, Liu Y, Long J, Chen S, Liao G, Wu S, Li C, Wang L, Ling W, Zhu H. Trimethylamine N-Oxide aggravates liver steatosis through modulation of bile acid metabolism and inhibition of farnesoid X receptor signaling in nonalcoholic fatty liver disease. Mol Nutr Food Res. 2019;63(17):e1900257.

23. Chu H, Duan Y, Yang L, Schnabl B. Small metabolites, possible big changes: a microbiota-centered view of non-alcoholic fatty liver disease. Gut. 2019;68(2):359–70.

24. Liu X, Tu J, Zhou Z, Huang B, Zhou J, Chen J. TMAO-Activated Hepatocyte-Derived Exosomes Are Widely Distributed in Mice with Different Patterns and Promote Vascular Inflammation. *Cardiol Res Pract* 2022, 2022:5166302.

25. Lin K, Wang X, Li J, Zhao P, Xi X, Feng Y, Yin L, Tian J, Li H, Liu X, et al. Anti-atherosclerotic effects of geraniin through the gut microbiota-dependent trimethylamine N-oxide (TMAO) pathway in mice. Phytomedicine. 2022;101:154104.

26. Chen S, Henderson A, Petriello MC, Romano KA, Gearing M, Miao J, Schell M, Sandoval-Espinola WJ, Tao J, Sha B, et al. Trimethylamine N-Oxide binds and activates PERK to promote metabolic dysfunction. Cell Metab. 2019;30(6):1141–e11511145.

27. Riva G, Villanova M, Cima L, Ghimenton C, Bronzoni C, Colombari R, Crestani M, Sina S, Brunelli M, D'Errico A, et al. Oil Red O is a useful Tool to assess Donor Liver steatosis on frozen sections during transplantation. Transpl Proc. 2018;50(10):3539–43.

28. Gill N, Dhillon B. RNA-seq data analysis for Differential expression. Methods Mol Biol. 2022;2391:45–54.

29. Anders S, Pyl PT, Huber W. HTSeq–a Python framework to work with high-throughput sequencing data. Bioinformatics. 2015;31(2):166–9.

30. Anders S, Huber W. Differential expression analysis for sequence count data. Genome Biol. 2010;11(10):R106.

31. Hu K. Become Competent in Generating RNA-Seq heat maps in one day for novices without prior R experience. Methods Mol Biol. 2021;2239:269–303.

32. Kanehisa M, Furumichi M, Sato Y, Kawashima M, Ishiguro-Watanabe M. KEGG for taxonomy-based analysis of pathways and genomes. Nucleic Acids Res. 2023;51(D1):D587–92.

33. Wu T, Hu E, Xu S, Chen M, Guo P, Dai Z, Feng T, Zhou L, Tang W, Zhan L, et al. clusterProfiler 4.0: a universal enrichment tool for interpreting omics data. Innov (Camb). 2021;2(3):100141.

34. Wiśniewski JR, Zougman A, Nagaraj N, Mann M. Universal sample preparation method for proteome analysis. Nat Methods. 2009;6(5):359–62.

35. Tyanova S, Temu T, Cox J. The MaxQuant computational platform for mass spectrometry-based shotgun proteomics. Nat Protoc. 2016;11(12):2301–19.

36. Sinitcyn P, Gerwien M, Cox J. MaxQuant Module for the identification of genomic variants propagated into peptides. Methods Mol Biol. 2022;2456:339–47.

37. Kanehisa M, Goto S. KEGG: kyoto encyclopedia of genes and genomes. Nucleic Acids Res. 2000;28(1):27–30.

38. Worley B, Powers R. PCA as a practical indicator of OPLS-DA model reliability. Curr Metabolomics. 2016;4(2):97–103.

39. Shannon P, Markiel A, Ozier O, Baliga NS, Wang JT, Ramage D, Amin N, Schwikowski B, Ideker T. Cytoscape: a software environment for integrated models of biomolecular interaction networks. Genome Res. 2003;13(11):2498–504.

40. Mitteer DR, Greer BD. Using GraphPad prism's heat maps for efficient, fine-grained analyses of single-Case Data. Behav Anal Pract. 2022;15(2):505–14.

41. Li Y, Ji X, Wu H, Li X, Zhang H, Tang D. Mechanisms of traditional Chinese medicine in modulating gut microbiota metabolites-mediated lipid metabolism. J Ethnopharmacol. 2021;278:114207.

42. Yang Y, Karampoor S, Mirzaei R, Borozdkin L, Zhu P. The interplay between microbial metabolites and macrophages in cardiovascular diseases: a comprehensive review. Int Immunopharmacol. 2023;121:110546.

43. Ding H, Liu J, Chen Z, Huang S, Yan C, Kwek E, He Z, Zhu H, Chen ZY. Protocatechuic acid alleviates TMAO-aggravated atherosclerosis via mitigating inflammation, regulating lipid metabolism, and reshaping gut microbiota. Food Funct 2024.

44. Huang Q, Zhang Y, Chu Q, Song H. The influence of polysaccharides on lipid metabolism: insights from Gut Microbiota. Mol Nutr Food Res. 2024;68(1):e2300522.

45. Swartz TH, Moallem U, Kamer H, Kra G, Levin Y, Mamedova LK, Bradford BJ, Zachut M. Characterization of the liver proteome in dairy cows experiencing negative energy balance at early lactation. J Proteom. 2021;246:104308.

46. Batista CP, Gonçalves RS, Contreras LVQ, Valle SF, González F. Correlation between liver lipidosis, body condition score variation, and hepatic analytes in dairy cows. Braz J Vet Med. 2022;44:e005121.

47. Lee E, Korf H, Vidal-Puig A. An adipocentric perspective on the development and progression of non-alcoholic fatty liver disease. J Hepatol. 2023;78(5):1048–62.

48. Bessone F, Razori MV, Roma MG. Molecular pathways of nonalcoholic fatty liver disease development and progression. Cell Mol Life Sci. 2019;76(1):99–128.

49. Ipsen DH, Lykkesfeldt J, Tveden-Nyborg P. Molecular mechanisms of hepatic lipid accumulation in non-alcoholic fatty liver disease. Cell Mol Life Sci. 2018;75(18):3313–27.

50. Alves-Bezerra M, Cohen DE. Triglyceride metabolism in the liver. Compr Physiol. 2017;8(1):1–8.

51. Fang C, Pan J, Qu N, Lei Y, Han J, Zhang J, Han D. The AMPK pathway in fatty liver disease. Front Physiol. 2022;13:970292.

52. Yan LS, Zhang SF, Luo G, Cheng BC, Zhang C, Wang YW, Qiu XY, Zhou XH, Wang QG, Song XL, et al. Schisandrin B mitigates hepatic steatosis and promotes fatty acid oxidation by inducing autophagy through AMPK/mTOR signaling pathway. Metabolism. 2022;131:155200.

53. Tanase DM, Gosav EM, Costea CF, Ciocoiu M, Lacatusu CM, Maranduca MA, Ouatu A, Floria M. The Intricate Relationship between Type 2 Diabetes Mellitus (T2DM), Insulin Resistance (IR), and Nonalcoholic Fatty Liver Disease (NAFLD). *J Diabetes Res* 2020, 2020:3920196.

54. Muzurović E, Mikhailidis DP, Mantzoros C. Non-alcoholic fatty liver disease, insulin resistance, metabolic syndrome and their association with vascular risk. Metabolism. 2021;119:154770.

55. Khan RS, Bril F, Cusi K, Newsome PN. Modulation of Insulin Resistance in nonalcoholic fatty liver disease. Hepatology. 2019;70(2):711–24.

56. Hosokawa Y, Hosooka T, Imamori M, Yamaguchi K, Itoh Y, Ogawa W. Adipose tissue insulin resistance exacerbates liver inflammation and fibrosis in a diet-induced NASH model. Hepatol Commun 2023, 7(6).

57. Zhang CY, Liu S, Yang M. Antioxidant and anti-inflammatory agents in chronic liver diseases: molecular mechanisms and therapy. World J Hepatol. 2023;15(2):180–200.

58. Qiu L, Feng R, Wu QS, Wan JB, Zhang QW. Total saponins from Panax japonicus attenuate acute alcoholic liver oxidative stress and hepatosteatosis by p62-related Nrf2 pathway and AMPK-ACC/PPARα axis in vivo and in vitro. J Ethnopharmacol. 2023;317:116785.

59. Kuka J, Liepinsh E, Makrecka-Kuka M, Liepins J, Cirule H, Gustina D, Loza E, Zharkova-Malkova O, Grinberga S, Pugovics O, et al. Suppression of intestinal microbiota-dependent production of pro-atherogenic trimethylamine N-oxide by shifting L-carnitine microbial degradation. Life Sci. 2014;117(2):84–92.

60. Zhang Y, Wang Y, Ke B, Du J. TMAO: how gut microbiota contributes to heart failure. Transl Res. 2021;228:109–25.

61. Coutinho-Wolino KS, de Oliveira Leal FCLFM, Mafra V, Stockler-Pinto D. Can diet modulate trimethylamine N-oxide (TMAO) production? What do we know so far? Eur J Nutr. 2021;60(7):3567–84.

62. Zhou S, Xue J, Shan J, Hong Y, Zhu W, Nie Z, Zhang Y, Ji N, Luo X, Zhang T et al. Gut-Flora-Dependent Metabolite Trimethylamine-N-Oxide Promotes Atherosclerosis-Associated Inflammation Responses by Indirect ROS Stimulation and Signaling Involving AMPK and SIRT1. *Nutrients* 2022, 14(16).

63. Li Q, Wu T, Liu R, Zhang M, Wang R. Soluble Dietary Fiber reduces trimethylamine metabolism via gut microbiota and co-regulates host AMPK Pathways. Mol Nutr Food Res 2017, 61(12).

64. Zhou B, Caudal A, Tang X, Chavez JD, McMillen TS, Keller A, Villet O, Zhao M, Liu Y, Ritterhoff J et al. Upregulation of mitochondrial ATPase inhibitory factor 1 (ATPIF1) mediates increased glycolysis in mouse hearts. J Clin Investig 2022, 132(10).

65. Jiang M, Zhang YX, Bu WJ, Li P, Chen JH, Cao M, Dong YC, Sun ZJ, Dong DL. Piezo1 channel activation stimulates ATP production through enhancing mitochondrial respiration and glycolysis in vascular endothelial cells. Br J Pharmacol. 2023;180(14):1862–77.

66. Steinberg GR, Hardie DG. New insights into activation and function of the AMPK. Nat Rev Mol Cell Biol. 2023;24(4):255–72.

67. Trefts E, Shaw RJ. AMPK: restoring metabolic homeostasis over space and time. Mol Cell. 2021;81(18):3677–90.

68. Xia T, Chen D, Liu X, Qi H, Wang W, Chen H, Ling T, Otkur W, Zhang CS, Kim J, et al. Midkine noncanonically suppresses AMPK activation through disrupting the LKB1-STRAD-Mo25 complex. Cell Death Dis. 2022;13(4):414.

69. Przygrodzka E, Hou X, Zhang P, Plewes MR, Franco R, Davis JS. PKA and AMPK Signaling pathways differentially regulate Luteal Steroidogenesis. Endocrinology 2021, 162(4).

70. Althaher AR. An Overview of Hormone-Sensitive Lipase (HSL). *ScientificWorldJournal* 2022, 2022:1964684.

71. Xu H, Lyu X, Guo X, Yang H, Duan L, Zhu H, Pan H, Gong F, Wang L. Distinct AMPK-Mediated FAS/HSL pathway is implicated in the alleviating effect of Nuciferine on obesity and hepatic steatosis in HFD-Fed mice. Nutrients 2022, 14(9).

72. Lee G, Kim YY, Jang H, Han JS, Nahmgoong H, Park YJ, Han SM, Cho C, Lim S, Noh JR, et al. SREBP1c-PARP1 axis tunes anti-senescence activity of adipocytes and ameliorates metabolic imbalance in obesity. Cell Metab. 2022;34(5):702–e718705.

73. Heeren J, Scheja L. Metabolic-associated fatty liver disease and lipoprotein metabolism. Mol Metab. 2021;50:101238.

## Publisher's note